Chalcogenide Letters Vol. 22, No. 12, December 2025, p. 999-1008

Density Functional Theory Analysis of the Electronic Properties of the $Ge_2Sb_2Te_5$

S.N. Garibova[1, 2], M. E. Aliyev[3], U. I. Ashurova[4], L. C. Suleymanova[4], A. M. Kerimova[1], S. A. Rzayeva[1], S. O. Guseynova[1], H. I. Novruzova[1], R. Z. Amirov[1] and F. Sarcan[5]

[1]Institute of Physics, Ministry of Science and Education of the Republic of Azerbaijan, Baku, 1073, Azerbaijan
[2]Department of Physics and Electronics, Khazar University, Baku, 1096, Azerbaijan
[3] Department of Electrical Engineering, Faculty of Engineering-Architecture, Nakhchivan State University, Nakhchivan, 7012, Azerbaijan
[4] Department of Energy, Faculty of Engineering, Mingachevir State University, Mingachevir, 4500, Azerbaijan
[5]Department of Physics, Faculty of Science, Istanbul University, Vezneciler, Istanbul, 34134, Turkey
*Corresponding Author: S. N. Garibova. Email: sqaribova1@gmail.com

Received: 05 September 2025; Accepted: 3 December 2025

ABSTRACT: In this work, the electronic behavior of the chalcogenide semiconductor $Ge_2Sb_2Te_5$ was examined using a first-principles computational approach. The study was carried out within the density functional theory framework, where the spin-polarized generalized gradient approximation was applied through the Atomistix ToolKit software. A double-zeta polarized basis set formed the foundation of the calculations, while exchange–correlation interactions were treated using the Perdew–Burke–Ernzerhof functional. Sampling of the Brillouin zone was performed according to the Monkhorst–Pack method with a 2 × 2 × 2 k-point grid, ensuring accuracy through special-point integration. Atomic configuration optimization, also conducted in Atomistix ToolKit, allowed the determination of the most energetically favorable arrangement for the Ge–Sb–Te lattice. Structural characteristics—including crystallite size and crystallinity—were evaluated using the Debye–Scherrer and Halder–Wagner analytical method. The relaxation of the unit cell revealed a marked redistribution of atoms, most notably between Ge and Te positions, resulting in higher symmetry and improved stability. Furthermore, the analysis indicated that distinct Ge–Sb–Te phases exhibit measurable differences in lattice constants, which in turn influence their physical performance. The refined structural model, characterized by enhanced symmetry and stability, provides a reliable representation of crystalline $Ge_2Sb_2Te_5$, making it a valuable reference for phase-change memory technology development.

KEYWORDS: First principle calculation; amorphous material; data storage elements; chalcogenide; spins generalized gradient approximation

1 Introduction

In modern electronics, the development of data storage devices is constantly improving. Today, many computers use solid-state drives with flash memory as storage, instead of volatile random-access memory [1]. The key advantage of this memory is that it keeps data when the power is off, although it usually works more slowly. One of the most common types of non-volatile memory is phase-change memory, often made from Ge–Sb–Te compounds [2]. In these materials, data storage works through a reversible change between the amorphous and crystalline states. This change happens when the active region is heated, allowing atoms in the memory cell to move [3]. During crystallization, many small crystal regions appear and disappear, creating random fluctuations. These fluctuations can be reduced if the entire volume crystallizes completely, which can be achieved with short voltage pulses lasting only a few nanoseconds. Once crystallized, the memory cell keeps its state even when the power, heat, or other energy sources are removed [4]. The phase change also changes the material's optical properties, such as absorption, reflectivity, and transmission. These effects are used in optical data storage systems [2,5–8]. The main goal is to achieve very fast crystallization, ideally in just a few picoseconds. One way to do this is by finding the most stable chemical composition.

https://doi.org/10.15251/CL.2025.2212.999

In this work, we study the electronic properties of the $Ge_2Sb_2Te_5$ using first-principles calculations to find a stable phase. Calculations were performed using density functional theory (DFT) with the spin-polarized generalized gradient approximation (SGGA). Atomic structure optimization and stable configuration searches were carried out using the Atomistix ToolKit (ATK) software package.

2 Experimental Detail and Discussion

Thin film samples with the 0.5 μm thickness of synthesized $Ge_{20}Sb_{20.5}Te_{51}$ compound were prepared by thermal evaporation onto glass substrates. These films were subsequently annealed at temperatures of 120, 220, and 400°C for 20 min [9]. X-ray diffraction (XRD) analysis of both film and bulk (~1 cm thickness) samples, before and after annealing, was performed using a Bruker D2 Phaser diffractometer with a CuKα radiation source (λ = 1.5406 Å). Structural characterization and data processing were conducted using the EVA and TOPAZ software packages [9].

The XRD spectrum of the film sample before annealing (Fig. 1) displays an amorphous halo-like profile prior to heat treatment (curve 1), without distinct diffraction peaks. In contrast, the bulk sample (curve 2) exhibits sharp and intense peaks, particularly near $2\theta \approx 30°$, indicating a well-developed crystalline structure. After annealing, a similar pattern of sharp peak formation is observed in the films, confirming crystallization. The broad band observed in curve 1 corresponds to the amorphous nature of the film. The degree of crystallinity (CI) for this sample was estimated to be 31% using the area-based method:

$$\mathrm{CI}(\%) = \frac{\mathrm{A_{cryst}}}{\mathrm{A_{cryst}} + \mathrm{A_{amorph}}} \times 100$$

A—Areas of the corresponding peaks.

Analysis of the XRD patterns and the calculated structural parameters (Table 1) indicate that the formation of a stable crystalline structure progresses as the annealing temperature increases from 120 to 400°C. The narrow peaks observed in bulk sample (curve 2) without heat treatment are largely reproduced in the film sample annealed at 220°C (curve 3), indicating a cubic structure. This structure corresponds to a metastable phase of the studied material. As the annealing temperature is raised to 400°C, the peak intensities of both film and bulk samples increase significantly. The data in Tables 1 and 2 show that samples annealed at 400°C exhibit the highest degree of crystallinity.

The film exhibits a gradual increase in crystallinity index from 31% to 72%, with crystallite sizes stabilizing at approximately 11 nm (Debye–Scherrer). In contrast, bulk samples initially possess high crystallinity (65%), reaching 100% at 400°C, accompanied by crystallite growth up to 25 nm. Halder–Wagner analysis shows very small, decreasing values (<1 nm) in films, whereas bulk samples increase from 5 to 10 nm. Annealing enhances crystallinity and enlarges crystallite dimensions in bulk samples. While the films are initially amorphous, they undergo gradual crystallization, yet retain relatively small crystallites. Different calculation yields divergent interpretations for thin films.

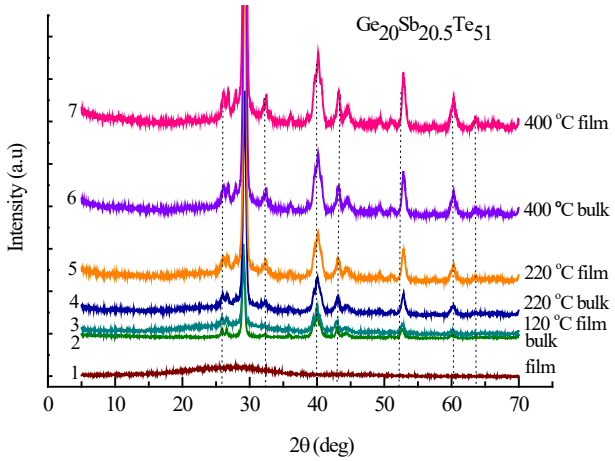

Figure 1: X-ray patterns of film and bulk $Ge_2Sb_2Te_5$ samples before and after heat treatment.

Table 1: Structure parameters of the $Ge_2Sb_2Te_5$ determined from XRD data.

Samples before and after Annealing	Crystallinity Index (CI, %)	Average Crystalline Size by Debye-Scherrer D (nm)	Average Crystalline Size by Halder-Wagner D (nm)
Film before	31	0.5	-
Film (120°C)	40	9.8	-
Film (220°C)	64	11	0.64
Film (400°C)	72	11	0.39
Bulk before	65	16	5
Bulk (220°C)	88	14	3
Bulk (400°C)	100	25	10

The Halder–Wagner model was used to study Ge-Sb-Te samples annealed at 200°C and 400°C by plotting $(\beta/\tan\theta)^2$ versus $(\beta/\tan\theta\sin\theta)$. Crystallite sizes were calculated from the slope [10]. In Fig. 2a, the data follow a clear linear relationship.

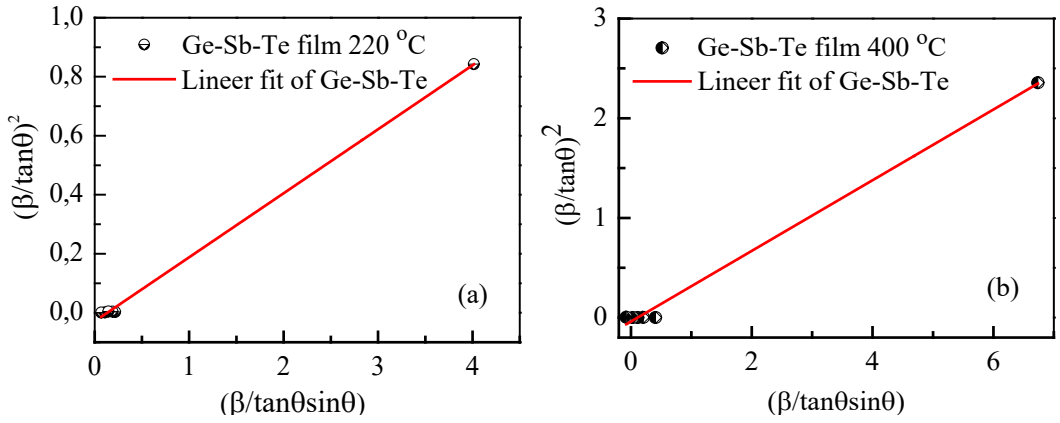

Figure 2: $(\beta/\tan\theta)^2$ versus $(\beta/\tan\theta\sin\theta)$ for Ge-Sb-Te films annealed at 200°C (**a**) and 400°C (**b**) using Halder-Wagner method.

The $(\beta/\tan\theta)^2$ values stay below ~1, showing that microstrains are small and crystallite size has little effect. In Fig. 2b, the linear relationship continues, but with higher $(\beta/\tan\theta)^2$ values, up to ~2.5, indi-

cating noticeable changes in the material at higher temperatures. The analysis shows that higher annealing temperatures increase crystallite size and reduce internal stresses, which strengthens the linear correlation.

The linear fit (Fig. 3a) exhibits a relatively small slope, which is indicative of comparatively large crystallite dimensions and low microstrain levels. By contrast, the pronounced increase in slope (Fig. 3b) corresponds to enhanced lattice distortions and a reduction in the average crystallite size following annealing at 200°C. The slope decreases again relative to the 200°C case (Fig. 3c), suggesting crystallite growth through recrystallization accompanied by a relaxation of internal stresses at higher annealing temperatures. Thus, annealing at 200°C facilitates microstrain accumulation and crystallite refinement, whereas annealing at 400°C (Fig. 3c) induces the opposite tendency—grain coarsening and stress relaxation.

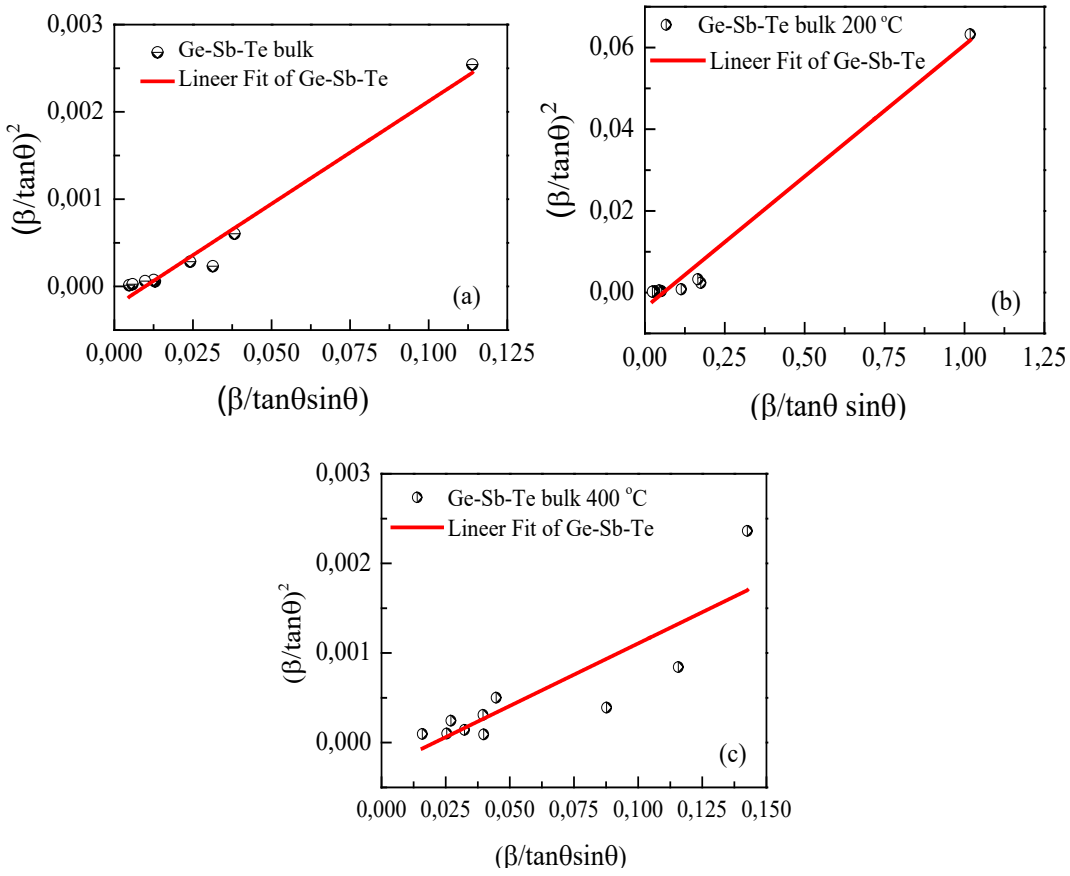

Figure 3: Halder-Wagner analysis of the Ge-Sb-Te bulk samples before and after annealing.

Table 2: Structure parameters of $Ge_{20}Sb_{20.5}Te_{51}$ evaluated by EVA and TOPAZ software from XRD.

Samples	Structure and Parameters (Å)	Volume (Å)	Density (g/cm^3)	d_{avg}-Value (Å)	Space-Group
Film (120°C)	Cubic, a = 5.997	215.68	6.220	3.8	Fm-3m (225)
Film and bulk (220°C)	Rhombo.H.axes, a = 4.189, c = 17.15	944.78	6.373	-	R-3m (166)
Film and bulk (400°C)	a = 4.189, c = 17.15	944.78	6.373	-	R-3m(166)

Fig. 4 presents the reflectance spectrum of a bulk $Ge_{20}Sb_{20.5}Te_{51}$ sample (~1 cm thickness) annealed at 200°C. Measurements were carried out using a Vertex 70v Fourier-transform spectrometer at an incidence

angle of 13°, under an atmospheric pressure below 100 Pa, in vacuum conditions, and at room temperature (300 K). The material exhibits a pronounced decrease in reflectance over the wavenumber range from 200 to 6000 cm^{-1}. In the low-frequency region (<1000 cm^{-1}), the reflectance reaches approximately 0.65; with increasing wavenumber, it gradually declines to about 0.15. This spectral behavior is characteristic of crystalline or partially crystallized materials containing free charge carriers, which is likely attributable to changes in the electronic structure induced by heat treatment.

The combined optical (IR spectroscopy) and structural (XRD) results therefore confirm the crystallization of $Ge_2Sb_2Te_5$ upon heating, accompanied by a significant change in reflectivity—an effect that should be taken into account when investigating phase transitions and in the design of phase-change materials based on this compound.

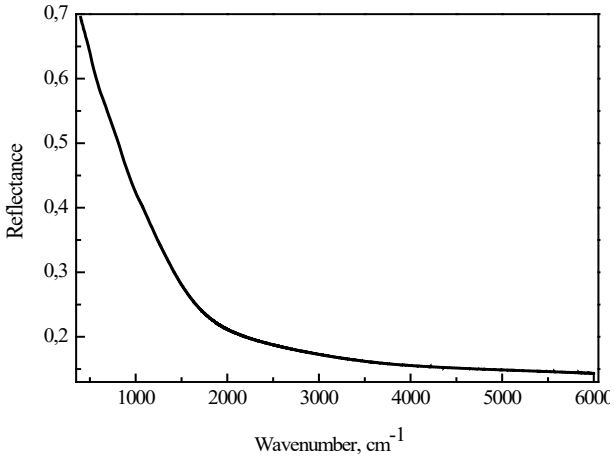

Figure 4: Reflectance spectrum of a bulk $Ge_2Sb_2Te_5$ sample annealed at 220°C.

3 Analysis using *Ab Initio* Simulation Method

This work examines the phase change of $Ge_2Sb_2Te_5$ (GST) using first-principles methods within the framework of density functional theory. The spin-polarized generalized gradient approximation was applied through the Atomistix ToolKit software package. The Atomistix ToolKit was employed to evaluate the energy spectra, electron density, atomic forces, transport and spin-dependent properties of $Ge_2Sb_2Te_5$ hexagonal phase. A Double Zeta Polarized (DZP) basis set together with the Perdew–Burke–Ernzerhof (PBE) functional was used to describe exchange–correlation interactions [11,12]. The structural optimization continued until the maximum atomic force was less than 0.01 eV/Å, and the largest stress tensor component dropped below 0.01 eV/Å³, ensuring fully relaxed lattice parameters. Brillouin zone sampling was carried out using the Monkhorst–Pack method with a 2 × 2 × 2 k-point grid, and the kinetic energy cutoff for wavefunction expansion was set to 150 Ry.

The investigated samples had lattice constants a = b = 4.2 Å, c = 17.15 Å, c/a = 4.08333, and b/a = 1. These parameters were obtained after annealing the material at 200 and 400°C (Table 2). Based on them, a primitive cell was constructed and visualized in Atomistix ToolKit before and after optimization. Fig. 5 presents the primitive cell geometry obtained from SGGA–DFT calculations, and Table 3 provides optimized $Ge_2Sb_2Te_5$ bond lengths for space group 221, along with comparisons to experimental values.

The optimization pathway included three main stages: the unrelaxed initial configuration (Fig. 5a), a partially optimized model (Fig. 5b) preserving P-3m1 symmetry (space group 164), and the fully relaxed structure (Fig. 5c) with Pm-3m symmetry (space group 221). The final configuration showed higher symmetry, improved energetic stability, and noticeable atomic rearrangements, especially involving Ge and Te atoms. In the visual model, Ge atoms appear as light orange spheres, Te atoms as blue, and Sb atoms as violet. The layered pattern, consisting of alternating Te and mixed Ge/Sb sheets, reflects the typical crystalline arrangement of GST materials.

These structural changes, particularly the repositioning of Ge and Te atoms, are significant for understanding how Ge–Sb–Te compounds transform between crystalline and amorphous states. Such transformations are central to their function in phase-change memory devices, where stability and symmetry of the crystalline phase are crucial for performance.

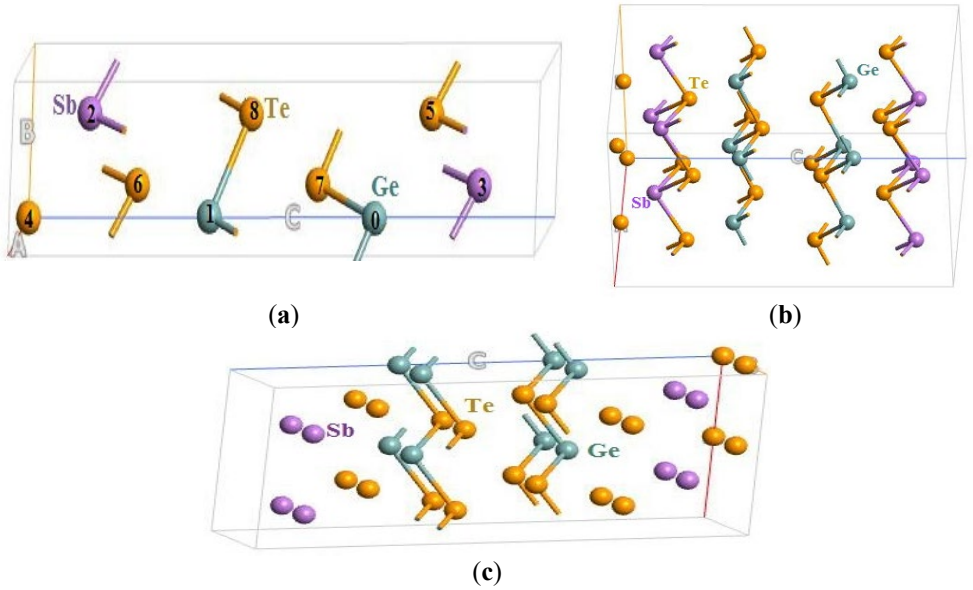

(**a**) (**b**)

(**c**)

Figure 5: Primitive cell of the $Ge_2Sb_2Te_5$ hexagonal structure calculated using SGGA before (**a**) and after atomic optimization (**b**,**c**) through the ATK software.

Table 3: Parameters of the polyatomic structure of the Ge-Sb-Te structure cell at (221).

Bond	SGGA—Bond Length (Å)	Experimental—Bond Length (±0.03 Å)	Deviation (Δ, Å)	Deviation (%)
Te_{17}–Ge_{10}	2.829	2.87	−0041	1.43
Te_7–Ge_0	2.77	2.77	0	0
Sb_2–Te_6	2.94	2.97	−0.03	1.01
Ge_1–Te_8	2.78	2.86–2.88	−0.09	3.14
Te–Sb	1.67	2.95–2.98	−1.295	43.68

Measurements of the lengths of short and long bonds as a function of temperature have previously been shown by some authors that the bond lengths are preserved upon transition to the high-temperature phase [13,14]. This means that the local structure of the high-temperature phase does not differ from the low-temperature phase. The bond lengths in the rhombohedral Ge-Te phase are 2.80 and 3.13 Å [15]. In the Ge-Te structure, there are many resonant bonds that can exist only in well-ordered structures [16], so in the amorphous phase, weak resonant bonds are broken and covalent bonds become more rigid [17], with the length of short bonds decreasing to 2.60 Å [15]. In the face-centered cubic phase $Ge_2Sb_2Te_5$, one lattice is occupied by Te atoms, and the second sub-lattice consists of Ge, Sb, and vacancies due to the lack of a sufficient number of valence electrons in Ge and Sb. Additional Ge or Sb atoms lead to the accumulation of atoms at grain boundaries rather than filling vacancies. Analysis of previously studied experimental works showed that in the face-centered cubic phase $Ge_2Sb_2Te_5$, the Ge-Te and Sb-Te bonds are divided into short and long [16]. The Ge-Te bond lengths are 2.83 and 3.2 Å, and the Sb-Te bond lengths are 2.91 and 3.2 Å [16]. Our calculated results (Table 3) with small deviations are in good agreement with the experimental results obtained by other authors [13–17].

Fig. 6 shows the optical spectra of the hexagonal phase of the $Ge_2Sb_2Te_5$ calculated within the linear response method for energies between 0 and 5 eV. The real (top panels) and imaginary (bottom panels)

parts of the dielectric permittivity tensor ε(ω) are presented for three components: ε_{xx}, ε_{yy}, and εzz. The real part, Re [ε(ω)], describes how the material absorbs light, while the imaginary part, Im [ε(ω)], relates to how it reflects light. Fig. 6a corresponds to the optimized (relaxed) primitive cell, and Fig. 6b shows the results before atomic positions were optimized.

For the relaxed structure (Fig. 6a), clear features appear between 1 and 3 eV, which correspond to electronic transitions between energy bands. In the unrelaxed case (Fig. 6b), both Re [ε] and Im [ε] are much higher, especially at low energies (<1 eV), indicating unrealistic behavior. Peaks in the imaginary part correspond to optical transitions and show the density of states above the band gap. After relaxation, these peaks shift and decrease in intensity, due to a lower density of states and a more stable electronic structure. The real part also becomes smoother and more physically reasonable.

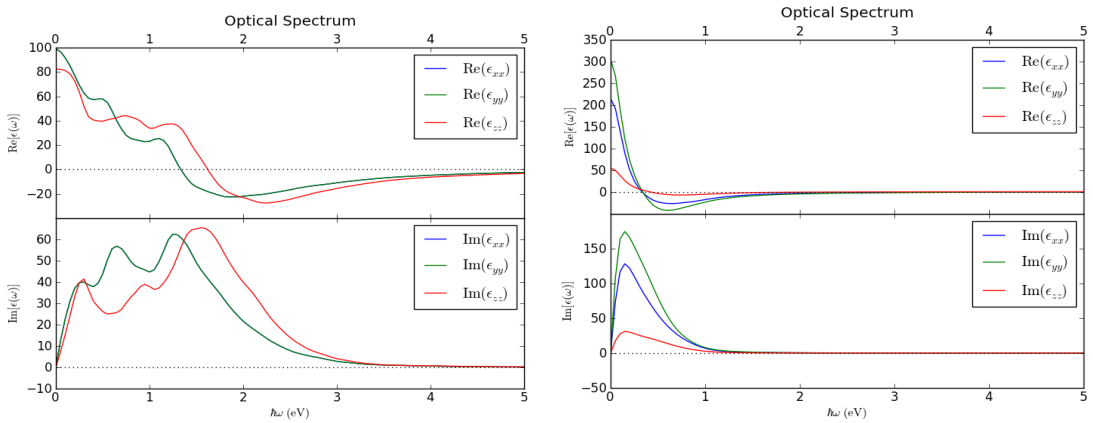

(**a**) (**b**)

Figure 6: Optical spectrum of the $Ge_2Sb_2Te_5$ hexagonal structure (real and imaginary parts of the permittivity tensor) plotted by ATK software; (**a**) primitive cell and (**b**) spectrum before optimization (relaxation) of atoms.

The ε_{xx} and ε_{yy} components are similar, as expected for hexagonal symmetry, while ε_{zz} differs noticeably, especially before relaxation. Overall, the spectra after optimization are more physically accurate and closer to experimental results.

Optimizing the positions of atoms has a strong impact on the material's optical properties. Relaxation reduces the imaginary part of the dielectric function and removes unstable features from the spectrum, showing that geometric optimization is essential before calculating optical properties. These changes are especially important for modeling photo-optical processes and for designing photonic and optoelectronic devices based on $Ge_2Sb_2Te_5$.

Fig. 7 depicts the computed electronic band structure of $Ge_2Sb_2Te_5$, derived using the SGGA. Incorporating spin polarization in the calculations enables the identification of potential magnetic-related features within the electronic structure. The *x*-axis displays high-symmetry points within the first Brillouin zone (such as Γ, M, L, A, K), which correspond to significant crystallographic directions. The *y*-axis represents the energies of electronic states (in eV), referenced with respect to the Fermi level, and indicated by a horizontal dashed line.

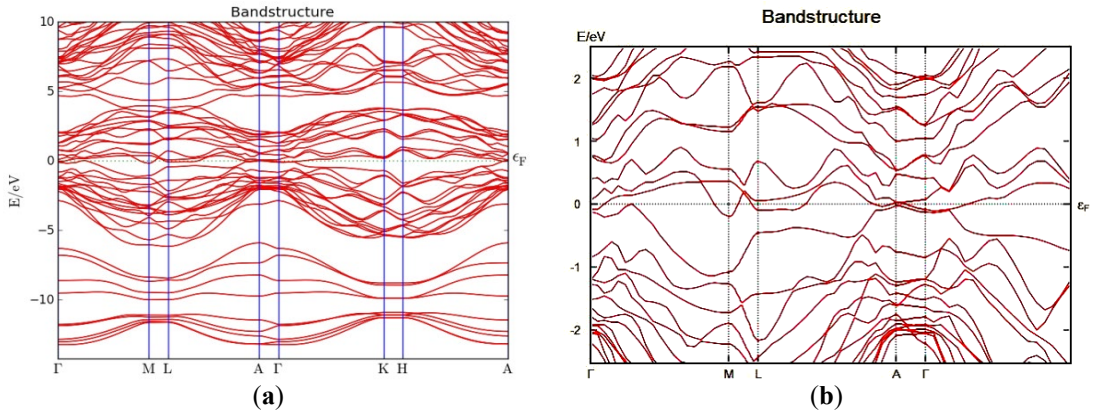

Figure 7: Electronic band structure of the $Ge_2Sb_2Te_5$ calculated using the SGGA and constructed through the ATK software.

Fig. 7a presents the electronic spectrum over −12 eV to +10 eV, encompassing both valence and conduction states, with the Fermi level marked by a dashed line. The visibly narrow gap suggests that $Ge_2Sb_2Te_5$ behaves as either a narrow-band gap semiconductor or a semimetal, depending on the Fermi level position. A high density of states below the Fermi level, dominated by Te, Sb, and Ge p-orbitals, is characteristic of complex chalcogenides.

Fig. 7b focuses on the −2 eV to +2 eV range near the Fermi level, revealing spin-resolved features. A small energy splitting, likely from exchange interactions or intrinsic spin polarization, is observed. The band separation is below 0.2 eV, supporting the material's semimetallic or narrow-gap semiconducting nature.

These results agree with prior reports noting the strong sensitivity of $Ge_2Sb_2Te_5$'s band structure to phase and computational method. The combination of a narrow gap and spin splitting highlights its potential for both phase-change memory and spintronic devices.

First-principles calculations place the Ge–Sb–Te band gap between 0.2 and 0.5 eV, consistent with semiconducting behavior. In the hexagonal phase, Te 5p orbitals dominate the valence band, while Ge 4p and Sb 5p states primarily forming the conduction band, indicating strong p–p orbital coupling.

Fig. 8 presents the total states density (black line) and the projected (partial) states density (red line) resolved by orbital character, highlighting the p-orbitals of Te and Sb atoms, which are typical for the valence band in chalcogenides. The contribution from s-states lies below −10 eV. The energy scale is referenced to the Fermi level (ε_F), indicated by the vertical dashed line at 0 eV.

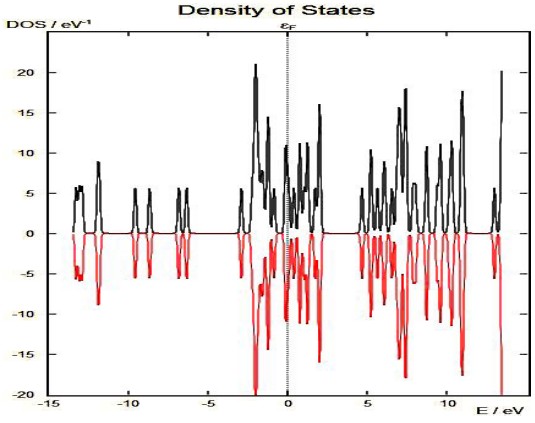

Figure 8: Total s- and p-state density of the hexagonal $Ge_2Sb_2Te_5$ structure constructed through the ATK software.

In the valence band region (left of ε_F), a pronounced state density is observed between −8 eV and 0 eV, dominated by the p-states of Te and Sb. In the conduction band (right of ε_F), the state density rises sharply immediately above 0 eV, indicating the absence of a wide band gap and suggesting semi-metallic behavior or a narrow-gap semiconducting character. The nonzero states density at ε_F is consistent with metallic or semi-metallic conductivity in the hexagonal phase of $Ge_2Sb_2Te_5$ often associated with crystallized phases containing defects or partial doping.

This observation aligns with experimental reflectance spectra and XRD results, which reveal crystallization upon heat treatment, accompanied by increased optical activity and electrical conductivity. The spin-up and spin-down components of the state's density are identical, confirming the antiferromagnetic nature of the material.

4 Conclusion

Density functional theory calculations with spin polarization using the Atomistix ToolKit software allowed a detailed characterization of the electronic structure and atomic configuration of the $Ge_2Sb_2Te_5$. Optimization of atomic positions based on XRD data for thin-film and bulk samples annealed at 200°C and 400°C demonstrated a significant impact on the material's optical properties. Geometric relaxation reduced the imaginary part of the dielectric function and eliminated unstable spectral features, confirming the importance of structural optimization prior to optical calculations.

Combined optical (IR spectroscopy) and structural (XRD) analyses revealed crystallization of the $Ge_2Sb_2Te_5$ upon heating, accompanied by changes in reflectivity, increased optical activity, and enhanced conductivity. Atomic redistribution, particularly of Ge and Te, led to higher symmetry and greater stability of the crystalline phase. Band structure and lattice parameter analysis showed that atomic ordering directly affects both electronic and structural properties. These results provide a reliable model of the crystalline phase of the $Ge_2Sb_2Te_5$, offering crucial insights into its phase transitions and supporting the development of next-generation phase-change memory devices.

Acknowledgement: Not applicable.

Funding Statement: The author (s) no specific funding for this study.

Author Contributions: The authors confirm contribution to the paper as follows: Idea, study conception and design: S.N.Garibova, A.M. Kerimova, F. Sarcan; data collection: M.E. Aliyev, S. A. Rzayeva, R.Z. Amirov; analysis and interpretation of results: S.N. Garibova, A.M. Kerimova, S. O. Guseynova, H. I. Novruzova, U. I. Ashurova, L. C. Suleymanova; draft manuscript preparation S.N. Garibova, A.M. Kerimova. All authors reviewed the results and approved the final version of the manuscript.

Availability of Data and Materials: Data available within the article and the data that support the findings of this study are available from the corresponding author, [S.N. Garibova], upon reasonable request.

Ethics Approval: Not applicable.

Conflicts of Interest: The authors declare no conflicts of interest to report regarding the present study.

References

1. Abou El Kheir O, Bonati L, Parrinello M, Bernasconi M. Unraveling the crystallization kinetics of the $Ge_2Sb_2Te_5$ phase change compound with a machine-learned interatomic potential. npj Comput Mater. 2024;10:33. https://doi.org/10.1038/s41524-024-01217-6.
2. Yamada N, Ohno E, Nishiuchi K, Akahira N, Takao M. Rapid-phase transitions of GeTe-Sb_2Te_3 pseudobinary amorphous thin films for an optical disk memory. J Appl Phys. 1991; 69(5): 2849–56. https://doi.org/10.1063/1.348620.
3. Feinleib J, de Neufville J, Moss SC, Ovshinsky SR. Rapid reversible light-induced crystallization of amorphous semiconductors. Appl Phys Lett. 1971;18(6):254–7. https://doi.org/10.1063/1.1653653.
4. Popescu M, Lőrinczi A, Sava F, Velea A, Matei E, Socol G, et al. Phase-change electrical memory elements and devices. J Optoelectron Adv Mater. 2008;10(10):2616–21.

5. Lacaita AL. Phase change memories: state-of-the-art, challenges and perspectives. Solid State Electron.2006; 50(1):24–31. https://doi.org/10.1016/j.sse.2005.10.046.
6. Redaelli A, Pirovano A, Benvenuti A, Lacaita AL. Threshold switching and phase transition numerical models for phase change memory simulations. J Appl Phys. 2008;103(11):111101. https://doi.org/10.1063/1.2931951.
7. Bogoslovskiy NA, Tsendin KD. Physics of switching and memory effects in chalcogenide glassy semiconductors. Semiconductors. 2012;46(5):559–90. https://doi.org/10.1134/S1063782612050065.
8. Raoux S, Welnic W, Ielmini D. Phase change materials and their application to nonvolatile memories. Chem Rev. 2010;110(1):240–67. https://doi.org/10.1021/cr900040x.
9. Garibova SN, Isayev AI, Rzayeva SA, Mammadov FN. Raman and X-ray diffraction data analysis of $Ge_2Sb_2Te_5$ films using Gaussian approximation considering the temperature population factor. Chalcogenide Lett. 2025;22(1):1–9. https://doi.org/10.15251/CL.2025.221.1.
10. Sarf F, Karaduman Er I, Yakar E, Acar S. The influence of annealing temperature on the gas sensing properties of multifunctional hematite (α-Fe_2O_3) films. J Mater Sci: Mater Electron. 2025; 36(3):187. https://doi.org/10.1007/s10854-025-14244-w.
11. Perdew JP, Wang Y. Accurate and simple analytic representation of the electron-gas correlation energy. Phys Rev B. 1992;45(23):13244. https://doi.org/10.1103/PhysRevB.45.13244.
12. Perdew JP, Burke K, Wang Y. Generalized gradient approximation for the exchange-correlation hole of a many-electron system. Phys Rev B. 1996;54:16533. Erratum in Phys Rev B. 1998; 57:14999. https://doi.org/10.1103/PhysRevB.54.16533.
13. Fons P, Kolobov AV, Krbal M, Tominaga J, Andrikopoulos KS, Yannopoulos SN, et al. Phase transition in crystalline GeTe: pitfalls of averaging effects. Phys Rev B. 2010; 82(15):155209. https://doi.org/10.1103/PhysRevB.82.155209.
14. Matsunaga T, Fons P, Kolobov AV, Tominaga J, Yamada N. The order-disorder transition in GeTe: views from different length-scales. Appl Phys Lett. 2011;99(23):231907. https://doi.org/10.1063/1.3665067.
15. Kolobov AV, Tominaga J, Frenkel AI, Ankudinov AL, Yannopoulos SN, Andrikopoulos KS, et al. Local structure of crystallized GeTe films. Appl Phys Lett. 2003;82:382–4. https://doi.org/10.1063/1.1539926.
16. Shprotko K, Kremers S, Woda M, Lencer D, Robertson J, Wuttig M. Resonant bonding in crystalline phase-change materials. Nature Mater. 2008:7;653–8. https://doi.org/10.1038/nmat2226.
17. Kolobov AV, Krbal M, Fons P, Tominaga J, Uruga T. Distortion-triggered loss of long-range order in solids with bonding energy hierarchy. Nature Chem. 2011;3(4):311–6. https://doi.org/10.1038/nchem.1007.